Micromechanical valve-operated needle-on-a-chip microinjection module for microfluidic large-scale integration

Delaney Gray-Scherr, ab Hudson Gasvoda, Alex Hadsell, Leilani Miller, Ebru Demir, e and I. Emre Araci. E

Ebru Demir, <u>demir@lehiqh.edu</u> Ismail Emre Araci, <u>iaraci@scu.edu</u>

Abstract

1

2

3

4

5

6

7

8

9

10

11

12

13

14

15

16

17

18

19

Microinjection is an essential process in genetic engineering that is used to deliver genetic materials into various biological specimens. Considering the high-throughput requirement for microinjection applications ranging from gene editing to cell therapies, there is a need for an automated, highly parallelized, reproducible, and easy-to-use microinjection strategy. Here we report an on-chip, microfluidic microinjection module designed for compatibility with microfluidic large-scale integration (mLSI) technology that can be fabricated via standard, multilayer soft lithography techniques. The needle-on-chip (NOC) module consists of a two-layer PDMS-based microfluidic module whose puncture and injection operations are reliant solely on Quake valve actuation. As a proof-of-concept, we designed a NOC module to conduct the microinjection of a common genetics model organism, *Caenorhabditis elegans* (*C. elegans*). The NOC design was analyzed using finite element method simulations for a large range of practically viable geometrical parameters. The computational results suggested that a slight lateral offset (>10 μm) of the control channel is sufficient for a successful NOC operation with a large fabrication tolerance (50 μm, 50% channel width). To demonstrate proof-of-concept, the microinjection platform was fabricated and utilized to perform a successful injection of a tracer dye into *C. elegans*.

Introduction

The development of high efficiency, automated cell transfection strategies has been a crucial requirement for applications ranging from assisted reproductive technology (e.g. IVF)^[1] and the generation of transgenic organisms (e.g. *C. elegans, drosophila, zebrafish*)^[2-8] to the optimization of genetic engineering technologies (e.g. RNAi, CRISPR/Cas9)^[2,3,9-13]. Cell transfection techniques are traditionally classified as either biological (e.g. viral transfection), chemical (e.g. lipofectamine), or physical (e.g. electroporation, microinjection) in nature^[2,14]. Of these strategies, physical, needle-based microinjection methods are attractive

a. Department of Bioengineering, Santa Clara University, Santa Clara, CA 95053, USA.

^{b.}Department of Biomedical Engineering, Boston University, Boston, MA 02215, USA.

^{c.} Department of Mechanical Engineering, Santa Clara University, Santa Clara, CA 95053, USA.

d. Department of Biology, Santa Clara University, Santa Clara, CA 95053, USA.

e. Department of Mechanical Engineering and Mechanics, Lehigh University, Bethlehem, PA 18015, USA.

^{*} Co-corresponding authors:

[†]Electronic Supplementary Information (ESI) available:

due to their versatility, reduced cell toxicity, and high delivery efficiency^[2,14,15]. However, while physical methods promise some of the best outcomes, they often require expensive, bulky equipment, and operation by a skilled technician^[2]. As a result, there have been several attempts in the literature to integrate physical microinjection with microfluidic technology—seeking to leverage the advantages of microfluidic platforms (i.e. high-throughput, small-scale, potential for simple automation and multiplexing)^[16-22] to improve injection speed, consistency, and user-friendliness.

The first significant attempt to develop a microneedle in a microfluidic platform was published by the Beebe group in 2003^[23]. By fabricating a PDMS- and glass-based device around the base of a microneedle they were able to control fluid ejection via microfluidic channel pressurization. This device allowed for precise control of liquid ejection but was not utilized for puncturing biological entities.

Current state-of-the-art microfluidic microinjection platforms have now evolved to include elements for the manipulation and immobilization of the injection target. In terms of injection mechanics, platforms typically either integrate mobile elements to shift the needle into an immobilized specimen^[24-28], or leverage flow dynamics and their resultant drag forces to direct the biological specimen onto a static needle.^[29-30] Adamo et al. employed the latter strategy, utilizing drag forces to maneuver and puncture individual cells against an embedded microneedle. In this case, the microneedle was connected to an external tube for ejection of the reagents^[29]. More recently, the Zappe group reported a pyrex and silicon-based microfluidic microinjector platform that included a microfluidic-integrated microneedle.^[30] Their microneedle was first fabricated using a surface micromachining process that incorporated silicon nitride structural layers and sacrificial phosphosilicate glass, before being integrated into deep reactive ion etched silicon channels.^[30] Then, much like in Adamo et al, fluidic drag forces were used to impale individual Drosophila embryos against the microfabricated microneedle.^[30] In both studies, external flow controllers were used to control the drag forces.^[29-30]

While these current microfluidic-based injection platforms *do* offer high efficiency and fully automated injections^[24-30], they rely on complex microfabrication strategies or depend on external elements such as micromanipulators to control microneedle movement, puncture, and reagent injection—thus, limiting platform miniaturization, portability, and potential for parallelization (i.e., compatibility with microfluidic large-scale integration (mLSI)^[16-20]). As such, there remains a need to develop a fully on-chip and integrated microinjection module with mLSI compatibility.

Here, we report the development of an on-chip, microneedle-based and micromechanical valve-operated microinjection module suitable for mLSI. The needle-on-chip (NOC) module consists of a two-layer PDMS-based microfluidic device that can be fabricated via standard, multilayer soft lithography techniques and its puncture and injection operations are reliant solely on Quake valve actuation. [16-20] The NOC module is also designed to be easily integrated with other PDMS-based microfluidic

modules (e.g. mixers, sorting arrays, etc.). To demonstrate proof of concept, we designed a NOC module to conduct microinjection of *Caenorhabditis elegans* (*C. elegans*), a common genetics model organism with a long history of microinjection. The *C. elegans* NOC microinjector design was first optimized using a 2D COMSOL simulation before being fabricated and utilized to perform a successful injection of tracer dye into *C. elegans* animals.

Materials and methods

Device design and dimensions

The complete *C. elegans* microinjection platform integrates both the NOC module and additional microfluidic modules inspired by Song et al (2016) (Fig. 1). The platform consisted of two PDMS layers bonded to a glass substrate: (1) the fluid-filled "flow" layer (bottom) where the *C. elegans* worms travel, and (2) the "control" layer (top) which exerts pneumatic valve control over the flow layer (Fig. 1A, 1B). Flow and control layer channels were 30 μm and 50 μm tall respectively and were separated by a 20 μm thick PDMS layer. The device consists of three essential regions: (i) a micropillar array, (ii) the NOC microinjection module, and (iii) multiple outputs for sorting animals post-injection (Fig. 1C). The micropillar array, designed to separate incoming worms and filter debris, contained micropillars 100 μm in diameter with 300 μm spacing. All flow layer channels downstream of the micropillar array (e.g. injection chamber, output channels) were rectangular channels 30 μm tall x 150 μm wide. The NOC microinjector reservoir is 600 μm in width, 30 μm in height, and 3 mm in length, holding ~50 pL of injection fluid. The PDMS membrane separating the microinjection reservoir from the worm channel is 40 μm thick. The microinjector needle, ~150 μm in length, with a tip width of ~3 μm is embedded in this membrane (see ESI†) and protrudes 5-10 μm into the worm flow channel. The microinjection reservoir was pressurized a 137 -207 kPa to expel fluid the needle into the worm flow channel.

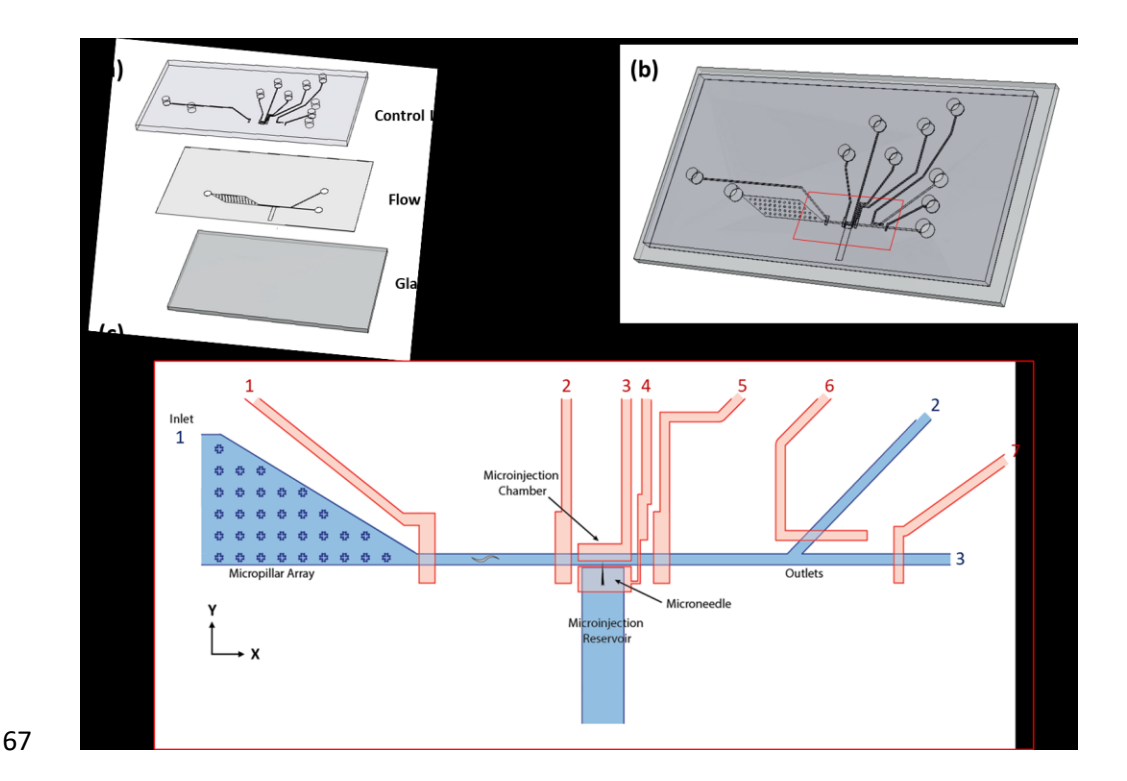


Figure 1. Schematic of microfluidic device design. (A) Exploded CAD model of 2-layer, PDMS-based microfluidic microinjection platform with *C. elegans*-specific NOC module. (B) Collapsed CAD model of microinjection platform. Red box outlines region of interest (ROI) shown in panel (C). (C) 2D schematic of ROI highlighting the fluidic input, micropillar array, NOC microinjection module, and fluidic outlets. Flow layer (blue), control layer (red). Blue numbers indicate flow layer fluid input (1) and outputs (2, 3). Red numbers (1-7) indicate control layer pneumatic inputs.

Device fabrication

The multilayer device was fabricated via standard photo and soft lithography techniques^[17-21]. Flow and control layer master molds were created via photolithographic patterning of SU-8 2050 negative photoresist (MicroChem) spin-coated to a thickness of 30 µm (flow layer) and 50 µm (control layer) (see ESI, Fig. S1). Master molds underwent tridecafluoro-1,1,2,2-tetra-hydrooctyl-1-trichlorosilane (TMCS, Santa Cruz Biotech) vapor treatment to prevent permanent PDMS adhesion to mold surface. To fabricate the flow layer, PDMS (RTV 615, RS Hughes) was mixed at a ratio of 20:1 (base-to-curing agent), degassed, spin-coated onto the flow layer mold at a thickness of 50 µm, and partially cured at 80°C for 1 hour. For the control layer, PDMS was mixed at a ratio of 5:1 (base-to-curing agent), poured over the control layer mold, degassed, and partially cured for 1 hour at 80°C. Partially cured control layer (PDMS 5:1) devices were then cut from the control master mold, pneumatic ports were punched (0.7 mm diameter), and control layer chips were aligned on top of the partially cured flow layer (PDMS 20:1). The aligned, partially cured chips were then allowed to permanently bond overnight at 80°C (i.e., off-ratio thermal bonding mechanism). Fully bonded chips were then cut from the flow mold and flow layer input/outputs were punched (1mm diameter). NOC microneedles were embedded into flow layer membrane (see detailed needle fabrication, insertion, and characterization in ESI† Fig. S2-S5 and Fig. 7) before

completed multilayer PDMS chips were bonded to glass microscope slides via air plasma surface activation. Pneumatic and fluidic access to device channels was provided by tubing connected via stainless steel pins inserted into inlet and outlet ports.

Design and operation of the Needle-on-chip (NOC) module for C. elegans-focused microinjection

The NOC microinjection module consists of two layers with the *C. elegans* injection specimen travelling laterally within the flow layer while pneumatically-operated, control-layer valves regulate worm immobilization and injection (Fig. 1C, 2). The microinjector reservoir chamber is located directly adjacent to the worm flow channel (Fig. 2). This chamber is separated from the worm channel by a thin PDMS membrane through which a microneedle tip is embedded (Fig. 2, S5). When the NOC microinjector reservoir chamber is filled with the desired injection fluid, it is pressurized to eject fluid through the needle into the worm flow chamber. To inject a worm, a control valve located directly above the animal is actuated to press the animal into the ejecting needle—simultaneously immobilizing and injecting the animal (Fig. 2C). Additionally, to prevent unwanted needle clogging or backflow from the worm channel, a valve above the microinjector reservoir can be actuated to seal off the microneedle's base when not in use (Fig. 2A, 2C).

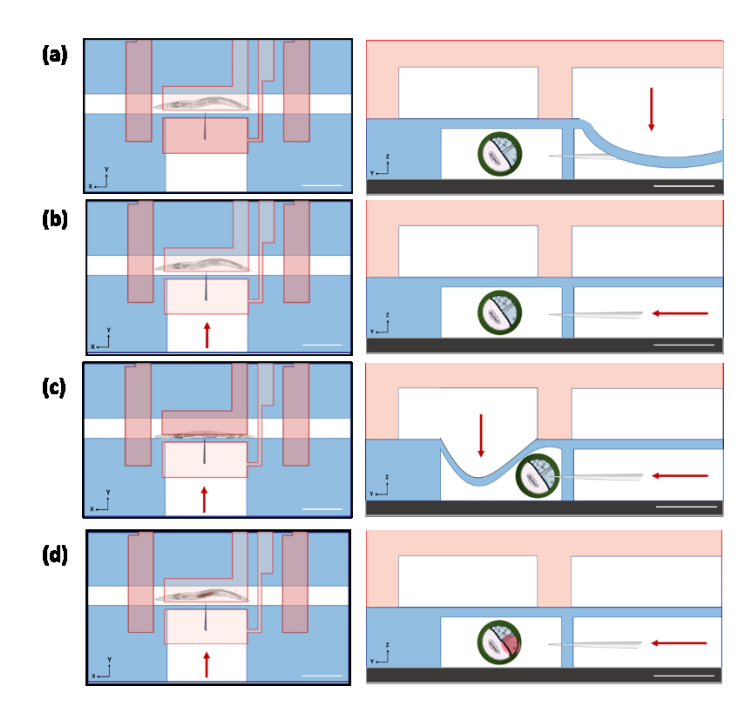


Figure 2. Needle-on-chip microinjector design and operation. Flow layer (blue), control layer (red), actuated valves (dark red). (Left column) Top-down view of worm trapped within flow layer microinjection module (scale bar is 300 µm). (Right column) Side view of worm trapped within flow layer microinjection module alongside embedded microneedle (scale bar is 50 μm). Injection steps: (A) Valve directly above microneedle base is actuated to prevent backflow while waiting for worm to get in position. (B) Valve above microneedle base is released and microinjection reservoir is pressurized to expel fluid into worm-containing flow channel. (C) Valve directly above worm body is actuated to press worm into fluid ejecting microneedle. (D) Valve directly above worm body is released while the microneedle is still ejecting fluid, thus completing the worm injection process.

2D Simulation of NOC module

87

88

89

90

91

92

93

94

95

96

97

98

99

100

101

102

103

The device is modeled in the 2D domain using the fluid-structure interaction module of the commercial software COMSOL Multiphysics, which fully couples the laminar flow and the solid mechanics modules, solving them simultaneously. The 2D model was operated for 1 mm unit thickness. The chip is modeled as a rectangle of dimensions 2500 μ m x 1000 μ m (x-direction vs. y-

direction unless otherwise stated) and made of polydimethylsiloxane (PDMS) (Fig.3A) Flow and control channels are modeled as rectangular chambers carved out of the large PDMS domain and are of dimensions 100 µm tall x 20 µm and 100 µm x 30 µm respectively (see Fig. 3A for model starting position). The control channel is positioned 20 µm above the flow channel to model the membrane thickness separating the flow and control layers, and the channels are positioned with a variable offset in x-direction. The flow channel has a 10 µm bottom wall thickness and its bottom wall is not allowed to deform, thus, mimicking the glass substrate. The left wall of the flow chamber is aligned with the vertical midline of the domain. The chambers are filled with water to mimic the physical characteristics of the fluid used in actual experiments. The *C. elegans* worm body was modeled as a disk (15 µm in radius), where the x-coordinate of the worm body's center coincides with the flow channel center when the x-offset of the control and flow channels are studied. Otherwise, it is studied as an additional variable. The worm body was modeled as nylon to mimic the elastic modulus of the worm's cuticle that would need to be punctured during an injection. While the elastic modulus of *C. elegans* of the cuticle and body has been reported to vary (e.g., age, mutants) ^[34]), nylon elastic modulus of 200 MPa that was used for our simulations falls within the range of reported cuticle measurements. It should also be noted that the numerical study reported here was not designed to be a high-fidelity simulation of the actual system, but rather an efficient method to rapidly screen NOC designs to help determine a range of geometric measurements that are most likely to yield a successful proof-of-concept microinjection.

To simulate the projected operation of the microinjector, the control channel is pressurized using boundary load boundary condition on the channel walls with a load of magnitude 137 kPa applied for 2 seconds. Contact is established between the worm and the flow channel walls using contact pairs so that any force resulting from the deformation of the channel would be transmitted to the worm. Force acting on the worm due to fluid movement inside the flow channel is neglected as it is found to be orders of magnitude smaller than the contact force. For the fluid domain, the P2+P1 discretization model in COMSOL is used, namely, second-order elements are used for the velocity components and linear elements are used for the pressure. Triangular mesh is used for the entire computational domain and boundary layer mesh is applied around the worm and channel walls. Moving mesh is applied to the channels to assure mesh element quality is preserved throughout the channel wall and worm movements. Mesh convergence of the simulations is verified by measuring the worm's velocity for increasing numbers of degrees of freedom (DOF) (i.e., for finer meshes). Increasing the number of DOF from 50000 to 162000 the velocity of the worm changed less than 3% whereas the computation time was 2.8 times higher. This error margin is found to be acceptable and the mesh with around 50000 DOF is used for the simulations reported in this study (Fig. S8). Time dependent solver with MUMPS direct solver (MUltifrontal Massively Parallel Sparse direct solver) is used in fully coupled mode with a time step of 0.01 ms.

Experimental platform

The experimental platform was composed of four elements: microfluidic microinjection platform, a positive pressure driven pneumatic multiplexor, a Leica dissecting scope, and a computer running both the Elveflow multiplexor controlling software and microscope software (Fig. S6A). The microfluidic device was secured to the stage of a Leica brightfield dissecting scope and the microinjector region was visualized at 10x. Fluid flow within the flow layer was manually controlled using a syringe. Control layer pneumatic valves and microinjector reservoir pressurization were controlled by a microfluidic multiplexer linked to Elveflow software.

Worm preparation and loading

All experiments utilized wild type N2 (Bristol) *C. elegans* obtained from the Caenorhabditis Genetics Center (CGC, University of Minnesota, MN). Standard techniques were used for maintenance and handling of *C. elegans* strains^[35]. Animals were grown at 20°C unless otherwise indicated. The animals described as wild-type were *C. elegans*, variety Bristol, strain N2^[35]. For optimal microinjection and the creation of a successful transformant, animals must be healthy, young adult hermaphrodites with a limited number of eggs. Age-synchronized populations were obtained using a standard hypochlorite solution (0.5 M NaOH, 1% NaClO) procedure^[36]. To prepare the chip for injection, the worm flow channel was filled with sterile M9 buffer (3 g KH₂PO₄, 6 g Na₂HPO₄, 5 g NaCl, 1 ml 1 M MgSO₄, H₂O per 1 liter) and the microinjection reservoir with a red dye to visualize injection. To load *C. elegans* into the device, animals were first rinsed off growth plates into 1.5 mL microcentrifuge using sterile M9 buffer. Next, they were drawn up into a 5mL syringe and loaded into chip via sterile tubing connected to the inlet adjacent to the micropillar array. A manually operated syringe connected via tubing to the device inlet was used to drive lateral animal progression through the flow layer. To unload animals, a tube was connected to the fluidic outlets and allowed to drip M9 buffer containing the worms onto a fresh growth media plate (Fig. S6A).

Results and Discussion

Computational evaluation of NOC *C. elegans* microinjector design

To evaluate the feasibility of our design, we built a 2D COMSOL model of the NOC module to determine: (1) whether this NOC design could successfully deflect a *C. elegans* worm into the wall containing the embedded needle, and (2) how variations in channel and worm position would affect injection parameters such as timescale, animal impact velocity, and max impact force. The 2D model consisted of a cross-sectional view of the PDMS-based NOC chamber, with a control valve located directly above

the flow channel containing the worm body (Fig. 3A). These flow and control layers were separated by a thin PDMS membrane that would deflect down into the flow channel upon application of a uniform pressure to the control channel. For the simulations, the following parameters were altered: (1) control valve offset from the flow channel, and (2) worm body position within the flow channel.

The first set of simulations placed the worm at the center of the flow channel and tested control channel offsets ranging from 0 to 80 μm to determine the range of flow and control layer alignments that could successfully deflect the worm into the injector wall (Fig. 3, 4). These results indicated that a control channel offset of at least 10 μm was required to deflect the worm laterally into the injector (Fig. 4b).

The maximum control channel offset that could successfully drive the animal to the injector wall was found to be 40 μ m, after which the membrane deflection down into the flow channel was significantly reduced (Fig. 4d). Without a control channel offset, the animal was simply compressed rather than deflected by the valve, as evidenced by oscillating force values but lack of lateral worm velocity (Fig. 4a). A successful wall impact is indicated by the sharp increase in force values seen in the -10, -20, and -40 μ m offset conditions (Fig. 4b-d).

Additionally, the positive force values recorded at the final time point (t=0.5 ms) in the -10, -20, and -40 μm offset conditions demonstrate that

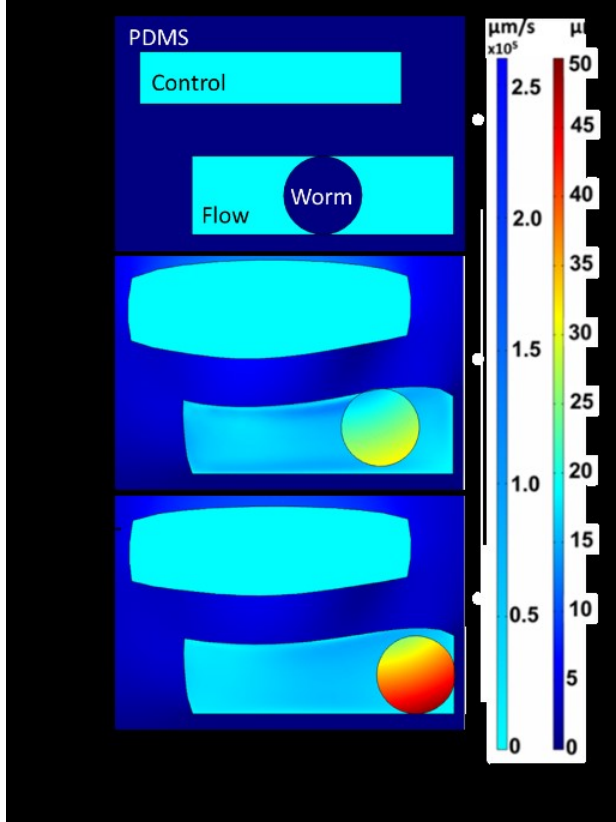


Figure 3. 2D computational NOC model and simulation of valve actuation to cause worm deflection in the -20 μm control channel offset condition. 2D model of the control channel (top rectangle, dimensions: 20 μm tall by 100 μm wide), flow channel (bottom rectangle, 30 μm tall x 100 μm wide), and worm cross-section (circle, 30 μm diameter). Control and flow channels separated by 20 μm thick PDMS. Dark blue regions outside of flow and control channels represent and were modeled as PDMS. Circle represents 2D cross-section of worm body modeled as a solid nylon circle (15 μm radius). Left color bar with 0-2.5 μm / sec scale shows the velocity of the liquid. Right color bar with 0-50 μm scale shows the displacement of all solids (PDMS, nylon worm body). (A) Model shown pre-valve actuation in its initial position. (B) Model immediately post-valve actuation. (C) Model immediately after worm contacts injector wall.

the actuated control valve continues to pin the worm against the injector wall beyond the moment of initial wall contact (Fig. 4b-d). With an offset higher than 40 μ m, the control valve was unable to successfully actuate to deflect the worm into the injector wall (Fig. 4e-f). This is observed in the - 60 μ m and -80 μ m offset conditions as an absence of substantial force and velocity measurements (Fig. 4e-f, M1 and M2 in ESI†). Based on these results, we concluded that the -20 μ m control channel offset resulted in the fastest time-to-impact (Fig. 4c, M3 in ESI†), closely followed by the -10 μ m offset condition (Fig. 4b).

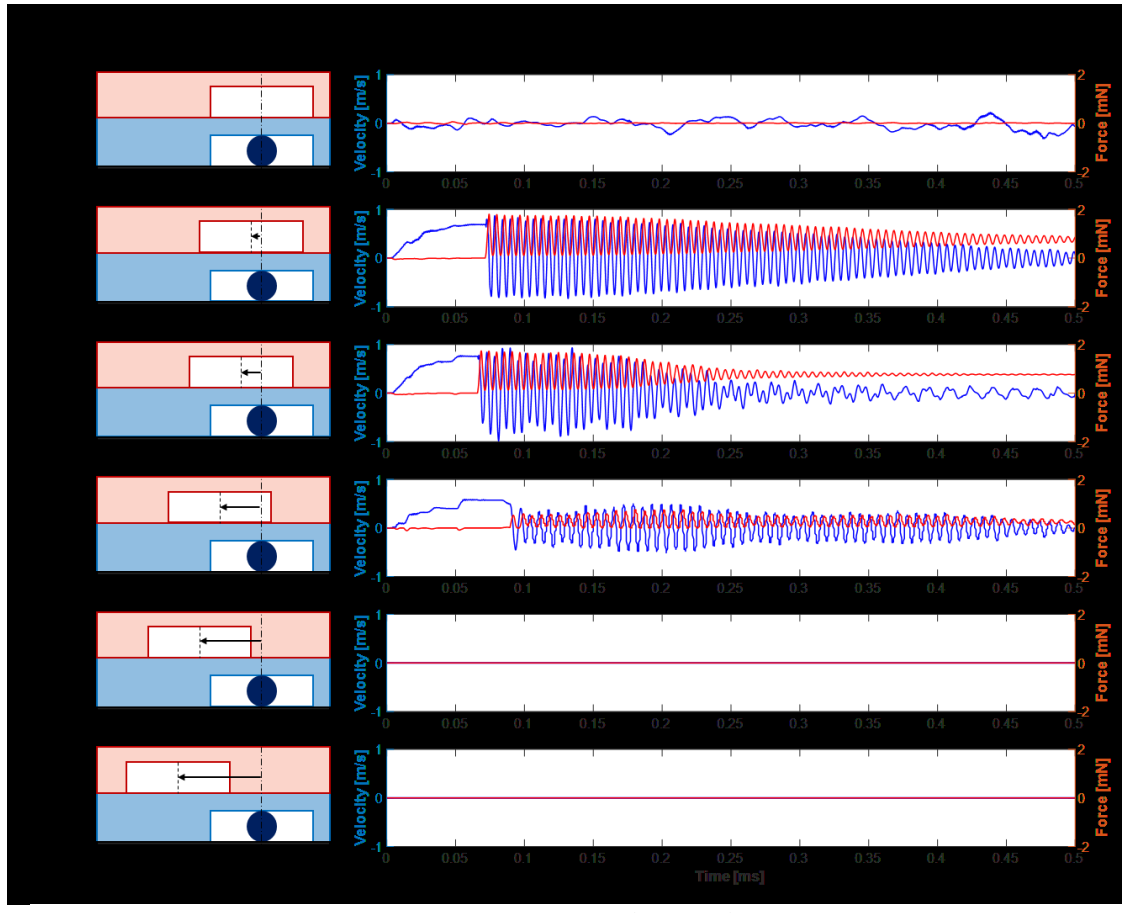


Figure 4. 2D Comsol Simulation of worm centered and control channel offset. (Left column) Worm position (black circle), flow layer (blue), control layer (red), glass slide (black base), and control layer valve (white box in red control layer). (Right column) Simulation results of worm velocity and experienced wall impact force as a product of control valve actuation (30psi) at t= 0 ms. Worm begins centered within flow channel in all conditions. Control channel offsets from central axis (dashed vertical line in left column) are as follows (A) 0 μm, (B) -10 μm, (C) -20 μm, (D) -40 μm, (E) -60 μm, (F) -80 μm.

Having identified the -20 μ m as an ideal valve offset for rapid worm deflection (Fig. 4b), we next studied the effect of offsetting the worm body from the central axis of the flow channel. These simulation results confirmed that the -20 μ m control channel valve offset could successfully deflect and pin the worm into the injector wall with worm body offsets of +10 μ m, 0 μ m, -10 μ m, and -20 μ m as evidenced by the sharp spikes in force and velocity upon impact, and the final positive pin force value at t = 0.5 milliseconds (Fig. 5). However, if the worm body was offset from the flow channel central axis beyond -20 μ m (i.e. -25 μ m, -30 μ m) the valve was unable to successfully deflect the worm into the injector wall (Fig. 5).

Upon confirming the -20 μm control channel offset could successfully deflect and pin worm bodies located within 75% of available worm positions (calculation in Appendix C and Fig. S7 of ESI†), we documented parameters from the -20 μm control channel offset condition relevant to injection speed and needle puncture—time-to-impact, worm body impact velocity, max worm body impact force, and the pin force experienced post-impact (Fig. 6).^[25-30]

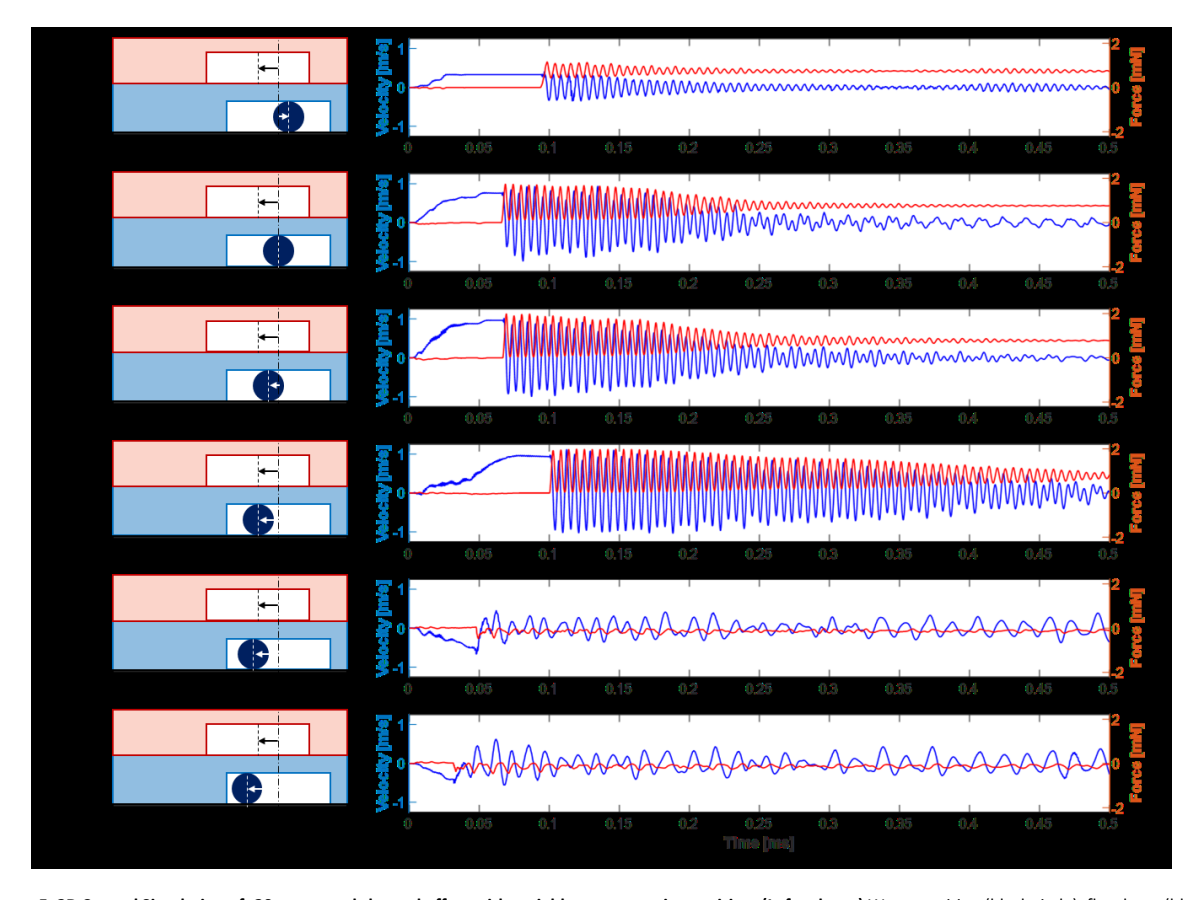


Figure 5. 2D Comsol Simulation of -20um control channel offset with variable worm starting position. (Left column) Worm position (black circle), flow layer (blue), control layer (red), glass slide (black base), and control layer valve (white box within control layer). (Right column) Simulation results of worm velocity and experienced wall impact force as a product of control valve actuation (30psi) at t=0 ms. Control channel offset is set to -20um in all conditions. Worm starting position offset from the central axis are as follows: (A) 10 um, (B) 0 um, (C) -10 um, (D) -20um, (E) -25um, (F) -30um.

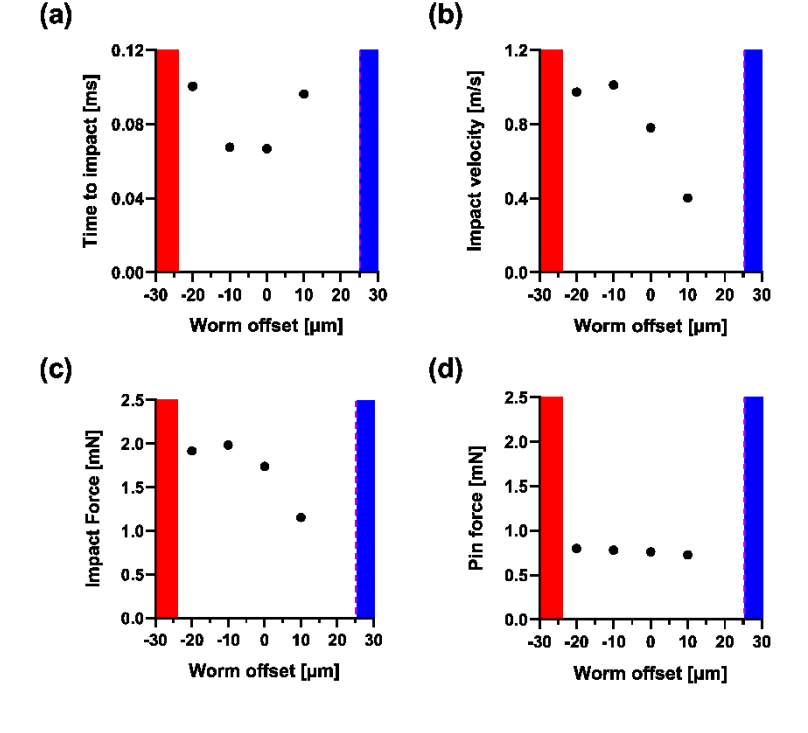


Figure 6. 2D Comsol Simulation, impact of worm position on injection specs for -20um control channel offset condition. Geometrically-limited maximum offset for worm position (purple), worm positions where worm is no longer deflected into injector wall (red). (A) Time taken for worm to hit injector wall post-valve deflection. (B) Worm's injector wall impact velocity. (C) Max force experienced by worm immediately after hitting injector wall. (D) Force experienced by worm after being held by valve against injector wall, data taken at t = 0.5 milliseconds.

In the -20 μ m control channel offset simulation, our results demonstrated that the worm body's impact velocity and impact force was highest when the worm body was positioned at a slight lateral offset (>10 μ m) from the control channel's central axis (Fig. 6b-c). As the worm body was positioned further from center of the actuated control valve (i.e. 0 and +10 μ m worm offset, Fig. 6b-c) the impact velocity and force decreased. This aligned with our prediction that the closer the animal was positioned with respect to the valve center, the faster it would be deflected into the injector wall. These results suggested that the -20 μ m control channel offset NOC design could deflect a worm located in a -25 and + 10 μ m offset position into the injector wall in under 0.1 ms. Finally, despite the variation in impact velocity and force, the pin force (measured at t = 0.5 ms) remained nearly constant across the simulations (Fig. 6d).

Evaluation of NOC microneedle fabrication and insertion feasibility

After using the computational model to validate that the mLSI- compatible NOC module could theoretically deflect a worm into the injector wall, we next sought to determine the feasibility of fabricating and embedding microneedles into the NOC module that were suitable for *C. elegans* microinjections. At a minimum, a suitable NOC microneedle would be perfusable with an open tip width of 3-6 μ m to minimize worm injury and ensure perfusability^[25]. It would also need to be embedded into the injector wall such that it protruded sufficiently into the worm flow channel to ensure it would reach the cytoplasmic region of the worm's gonadal arm during an injection. In general, a young adult *C. elegans* hermaphrodite (appropriate age for injection) has a diameter of about 50 μ m^[37]. The distal arm of its gonad is approximately half the worm's total diameter, making it about 25 μ m in length. To aim for a needle penetration depth that would fall within the cytoplasmic region of the gonad, the NOC microneedle would need to protrude into the worm flow channel at least 6 μ m to pass the worm cuticle, but no more than ~20-25 μ m to avoid rupturing the far wall of the gonad and losing injection fluid or potentially killing the animal. After fabricating microneedles via standard protocols employed in manual *C. elegans* microinjections^[5], we confirmed that we could consistently generate

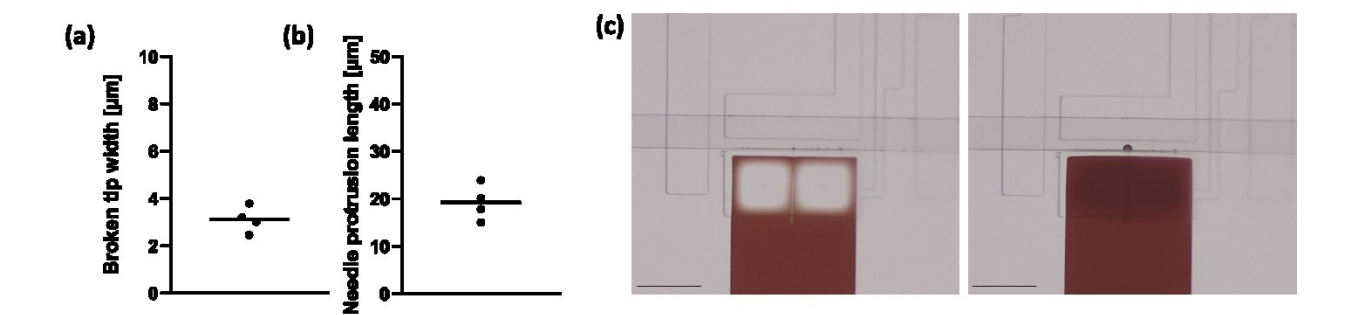


Figure 7. NOC Embedded microneedle characterization. (a) Outer diameter of open microneedle tip used in NOC module (n=4, bar represents mean). (b) Length of NOC embedded needle that protrudes out into worm flow channel (n=4, bar represents mean). (c) Perfusability test of embedded microneedle in NOC module (scale bar = 300 μm) (Left) Prior to 30 psi pressurization of NOC microinjector reservoir filled with red tracer dye. Control valve located above microneedle is pressurized to prevent backflow from flow channel. (Right) Time = 0.16 seconds post-pressurization of NOC microinjector reservoir.

microneedles with a broken, perfusable tip with an acceptable outer diameter of $3.12 \pm 0.55 \,\mu m$ (n=4) (Fig. 7a, S2). To evaluate the feasibility of embedding microneedles into a PDMS membrane within the microfluidic chip, we fabricated a physical version of the NOC module, manually cut off microneedle tips and embedded them into the NOC injector wall (Appendix B and Fig. S2-S5 in ESI). We confirmed that we could consistently embed the microneedles such that they protruded a depth of $19.27 \pm 3.77 \,\mu m$ (n=4) into the worm flow channel (Fig. 7b, S5), a value well within our range of acceptable protrusion lengths. We also confirmed that the newly embedded microneedle tips retained their perfusability as demonstrated by the successful ejection of red tracer dye shown in Fig. 7c.

NOC design validation and successful operation

Having utilized the 2D computational simulation to determine the ideal NOC design and validated the feasibility of fabricating and embedding the NOC microneedle, we next built a microfluidic NOC chamber with dimensions based on the simulation results to experimentally validate the injection mechanism's feasibility and confirm NOC's compatibility with other microfluidic modules. Our device design, based upon Song et al (2016) consisted of three core modules: (i) a micropillar array used to separate incoming worms and filter debris, (ii) the NOC module, and (iii) outputs (Fig. 1). The NOC module integrated into the chip consisted of a flow channel (30 µm tall, 100 µm wide) and a control channel (50 µm tall) separated by a 20 µm thick PDMS membrane. Along the length of the NOC injection module runs a microinjector reservoir that holds the injection fluid of interest. Separating this microinjection reservoir from the worm flow channel is a PDMS membrane (40 µm thick) containing an embedded microneedle protruding into the flow channel. An additional control valve was added directly above the microinjection reservoir chamber that could be actuated to prevent flow through the needle – a precaution against backflow from the flow channel into the reservoir or unwanted leakage of injection fluid into the flow channel. As in the simulations, the NOC control valve located

To conduct an injection, the worm flow channel was pre-filled with sterile M9 buffer and the NOC microinjector reservoir with a red tracer dye to visualize injection. Age-synchronized *C. elegans* animals were then loaded into the inlet connected to the micropillar array (Fig. 1C, inlet 1). Once in the chip, animals were driven through the micropillar array until they reached actuated control valve 1 (Fig. 1C), which was kept actuated by default to prevent a high number of animals from progressing through to the NOC module. Control valve 1 was released and then immediately re-actuated to allow a single animal to pass through and progress to the NOC injection module. The released animal continued to move along the flow channel until it was stopped by actuated control valve 5, located at the far end of the NOC injection chamber (Fig. 1C). Control valve 2 was then actuated to trap the animal alongside the microinjection reservoir located between control valves 2 and 5 (Fig. 1C). To perform the injection, the

directly above the flow channel was designed to deflect the animal into the injector wall upon its actuation - serving to

simultaneously pin the animal in place and puncture it against the microneedle.

microinjection reservoir was pressurized (30psi) to begin expelling injection fluid into the flow channel (M4 in ESI†). NOC control valve 3 (Fig. 1C) was then actuated, as in the simulations, to deflect the worm into the injector wall--simultaneously pinning and puncturing the worm against fluid-ejecting microneedle. As the simulations predicted, an animal located at a worm offset position of 10 µm was successfully deflected into the injector wall by a control channel valve that was offset by -10 µm (Fig. 4B). Additionally, the valve deflection and pin force proved sufficient to successfully puncture animal against the protruding microneedle. Interestingly, despite the successful puncture of the animal with the fluid-ejecting needle, no tracer dye was seen entering the animal body while the NOC control valve 3 was actuated. However, upon release of control valve 3, red dye could be seen entering the animal's body as it slid off the needle (Fig. 8, M4 in ESI†). We confirmed that the dye had successfully entered and been retained within the worm body by flushing M9 buffer around the animal (Fig. 8, M4 in ESI†). The animal's cuticle remained intact and the animal survived the injection process. These results offer a promising, experimental proof-of-concept of the NOC module's injection capacity and compatibility with *C. elegans* microinjections.



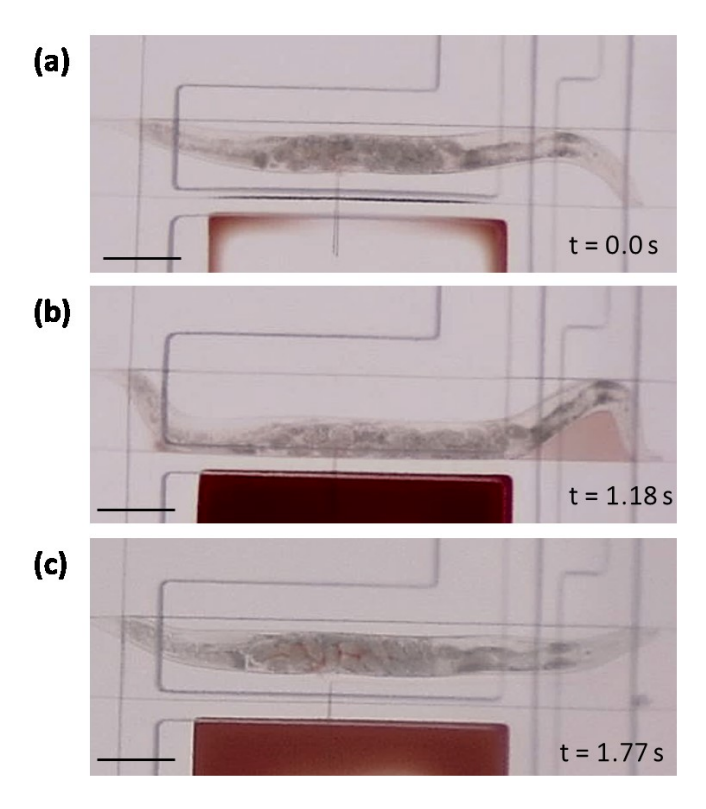


Figure 8. Injection of tracer dye into *C. elegans* using novel on-chip microinjector. Images taken from video M4 in ESI†. Dye injection lasts 0.28 seconds. Scale bars (A-C) are 150 μm. (A) Pre-injection. Adult worm trapped in microinjector region with control valves 2 and 5 actuated. (B) Midlijection. Control valve 3 located directly on top of worm is actuated to immobilize and press worm into the fluid-ejecting needle tip. (C) Post-injection. Red tracer dye can be seen inside of worm body.

Conclusions

Here we report the design and fabrication of an mLSI-compatible, on-chip microinjection module. The needle-on-chip (NOC) injector consists of a two-layer PDMS-based microfluidic module that can be fabricated via standard, multilayer

soft lithography and was designed to be easily automated and integrated with computer-guided operation. [28]

The NOC microinjector design offers a number of key advantages that distinguish it from previous microfluidic microinjectors: (1) it requires no external manual microinjector setup, (2) the specimen puncture and injection operation rely solely upon Quake valve actuation by a standard positive pressure source, it allows for (3) integration with other components in the mLSI toolbox, and thus, (4) offers the potential for injection parallelization.

The core concept of the NOC microinjection module was to utilize micromechanical pneumatic valve actuation to drive a biological specimen into an embedded microneedle. To assess the theoretical feasibility of using simple valve actuation to deflect and puncture the worm against a microneedle, we first built a 2D computational simulation of the NOC worm deflection operation. It should be noted that the numerical study reported here was not designed to be a high-fidelity simulation of the actual system, but rather, an efficient method to rapidly screen NOC designs and determine the range of micromechanical valve positions most likely to yield a successful proof-of-concept microinjection. The simulation's ability to predict an effective NOC geometry and specify its design tolerance was later confirmed by the successful proof-of-concept injection (Fig. 8).

The simulation was also utilized to predict the injection timescale (Fig. 6, time-to-impact metric), confirming that a NOC injection could be executed on timescales comparable, if not faster, than current published *C. elegans* injection speeds. Current state-of-the-art microfluidic microinjectors report injection speeds of approximately 9 seconds per worm, which includes the processes of worm loading, immobilization, injection, and release^[27,28]. At the other end of the spectrum, manual microinjection takes 2-4 minutes per worm for an experienced injector^[38]. Our simulation "time-to-impact" results indicated that our NOC design with a -20 µm control channel offset was capable of pushing a 30 µm diameter worm into the injector wall within 0.067 to 0.101 milliseconds. While we acknowledge that these data reflect "time to impact" rather than a complete injection sequence (i.e. loading, immobilization, injection, unloading), these results are encouraging given that our NOC module efficiently combines two injection steps – immobilization and injection. While we lacked advanced cameras or sensors in this study to precisely document the worm deflection velocity or time-to-impact in our experimental system, we were able to qualitatively confirm the rapidity of the worm deflection event and with our limited camera frame rate, determine that both the deflection of the worm into the injector wall was complete within 32 milliseconds (see ESI, M4).

Finally, the simulation yielded additional data on parameters proposed to be relevant to *C. elegans* injection performance: post-deflection worm velocity and wall impact force. While this proof-of-concept experimental study lacked the camera speed to quantify these parameters experimentally and was not adequately powered to characterize

the impact of these parameters on injection survival, previous work in the fields of cell microinjection and puncture dynamics has indicated that needle impact velocity and puncture force correlate with injection site deformation and potential damage^[25-30]. As such, we have included this potentially important and previously unreported *C. elegans* injection simulation data and propose that future work should explore the relationship between impact velocity and force *C. elegans* injection success. Additionally, it is worth noting it might also be possible to reduce animal injury upon needle puncture by adjusting the microneedle pulling parameters to alter the microneedle taper and tip dimensions.

Having identified an ideal NOC geometry using the simulation results, the selected NOC design was fabricated and integrated in sequence with other microfluidic modules (Fig. 1C). In a proof-of-concept experiment, we successfully used the NOC module to inject a tracer dye into a *C. elegans* animal. While this injection would not have yielded transgenic offspring because it injected the worm uterus rather than one of the two-armed gonadal syncytia, the NOC embedded microneedle could be shifted slightly along the X-axis to target the off-center gonadal arms. Additionally, to increase injection success rate, the NOC design could be adapted to integrate two off-center embedded microneedles to intentionally target both gonadal arms. To obtain successful transformants, these injections would need to be performed on young-adult hermaphrodites because the successfully injected worm (Fig. 8) was fully mature. However, despite these limitations, the NOC module successfully injected tracer dye into the body of a *C. elegans* worm and yielded no obvious animal leakage or injury, thus reinforcing the NOC module's promise as a viable microinjection design.

Finally, it is important to note that the reported NOC microneedle fabrication and embedding is a manual process. Although, we were able to obtain functional NOC modules and relatively consistent needle dimensions (Fig. 7) with this technique, the requirement of a skilled technician is an obstacle against mass scale manufacturability. It can be argued that in an industry setting this fabrication process and embedded needle placement could be streamlined to dramatically improve NOC consistency and precision. This could enable manufacturing of the required NOC designs for a wide range of injection specimens (i.e. single cell, drosophila) and allow for easier integration with computer-guided automation to achieve highly parallel microinjection operations.

Author Contributions

D.G.-S.: Conceptualization, methodology, investigation, data collection, data analysis, and writing and review of original manuscript. **H.G.:** Simulation methodology, simulation investigation, simulation data collection, and review of manuscript. **A.H.:** Conceptualization, methodology, investigation, data collection, and review of manuscript. **L.M.:** Conceptualization, resources,

321 and review of manuscript. E.D.: Simulation conceptualization, methodology, investigation, data collection, and review of 322 manuscript. I.E.A.: Supervision, resources, conceptualization, methodology, and writing and review of original manuscript. **Conflicts of interest** 323 324 There are no conflicts to declare. Data availability statement 325 326 All data generated or analyzed during this study are either included in this published article (and its supplementary 327 information files) or available upon reasonable request from the authors. **Funding statement** 328 329 This study was supported by and carried out under Santa Clara University School of Engineering's Senior Design 330 Program. **Ethics statement** 331 332 Per the Animal Care and Use Committee guidelines, no approval was needed for C. elegans work as it is an invertebrate. 333 Acknowledgements 334 We would like to thank Santa Clara University's (SCU) School of Engineering for funding this project. Additional thanks 335 SCU's Center for Nanostructures and SCU's Biology Department for providing fabrication facilities and support. References 336 337 338 1 R.C. Sequeira, T. Criswell, A. Atala, and J.J. Yoo, Tissue Engineering and Regenerative Medicine, 2020, 17.6, 787-800. 339 2 M.P. Stewart, R. Langer, and K.F. Jensen, *Chemical reviews*, 2018, **118.16**, 7409-7531. 340 3 J.M. Meacham, K. Durvasula, F. L. Degertekin, and A.G. Fedorov, Journal of laboratory automation, 2014, 19.1, 1-18. 341 4 H. Hwang, and H. Lu, Biotechnology journal, 2013, 8.2, 192-205.

- 342 5 C. Mello, and A. Fire, *Methods in cell biology*, 1995, **48**, 451-482.
- 343 6 V. Praitis, and M.F. Maduro, *Methods in cell biology*, 2011, **106**, 159-185.
- 344 7 E.A. Wimmer, *Nature reviews genetics*, 2003, **4.3**, 225-232.
- 345 8 Y. Zhao, H. Sun, X. Sha, L. Gu, Z. Zhan, and W.J. Li, *Micromachines*, 2018, **10.1**, 7.
- 346 9 A. Fire, S. Xu, M.K. Montgomery, S.A. Kostas, S.E. Driver, and C.C. Mello, *Nature*, 1998, **391.6669**, 806-811.
- 347 10 H. Tabara, A. Grishok, and C.C. Mello, *Science*, 1998, **282.5388**, 430-431.
- 348 11 T.-W. Lo, C.S. Pickle, S. Lin, E.J. Ralston, M. Gurling, C. M. Schartner, Q. Bian, J.A. Doudna, and B.J. Meyer, Genetics,
- **349** 2013, **195.2**, 331-348.
- 350 12 S. Xu,. Journal of Genetics and Genomics, 2015, **42.8**, 413-421.
- 351 13 H.-X. Wang, M. Li, C.M. Lee, S. Chakraborty, H.-W. Kim, G. Bao, K. W. Leong, *Chem. Rev.*, 2017, **117**, 9874–9906.
- 352 14 B. Duckert, S. Vinkx, D. Braeken, and M. Fauvart, Journal of Controlled Release, 2021, 330, 963-975.
- 15 S. Permana, E. Grant, G.M. Walker, and J.A. Yoder, IEEE/ASME Transactions on Mechatronics, 2016, 21.5, 2391-2404.
- 354 16 M.A. Unger, H.-P. Chou, T. Thorsen, A. Scherer, and S.R. Quake., *Science*, 2000, **288.5463**, 113-116.
- 355 17 T. Thorsen, S.J. Maerkl, and S.R. Quake, *Science*, 2002, **298.5593**, 580-584.
- 356 18 T.M. Squires, and S.R. Quake., Reviews of modern physics, 2005, 77.3, 977.
- 357 19 I.E. Araci, and S.R. Quake, *Lab on a Chip*, 2012, **12.16**, 2803-2806.
- 358 20 I.E. Araci, and P. Brisk., *Current opinion in biotechnology*, 2014, **25**, 60-68.
- 359 21 E.K. Sackmann, A.L. Fulton, and D.J. Beebe, *Nature*, 2014, **507.7491**, 181-189.
- 360 22 K.F. Sonnen, and C.A. Merten, *Developmental cell*, 2019, **48.3**, 293-311.
- 361 23 S. Lee, W. Jeong, and D.J. Beebe., *Lab on a Chip*, 2003, **3.3**, 164-167.
- 362 24 A. Noori, P.R. Selvaganapathy, and J. Wilson., Lab on a Chip, 2009, 9.22, 3202-3211.
- 363 25 R. Ghaemi, J. Tong, B.P. Gupta, and P.R. Selvaganapathy, Micromachines, 2020, 11.3, 295.
- 364 26 X. Zhao, F. Xu, L. Tang, W. Du, X. Feng, and B.-F. Liu, Biosensors and Bioelectronics, 2013, 50, 28-34.
- 365 27 P. Song, X. Dong, and X. Liu, *Biomicrofluidics*, 2016, **10.1**, 011912.
- 366 28 X. Dong, P. Song, and X. Liu, *IEEE Transactions on Automation Science and Engineering*, 2020, **18.2**, 850-859.
- 367 29 A. Adamo, and K.F. Jensen., *Lab on a Chip*, 2008, **8.8**, 1258-1261.
- 368 30 D. Delubac, C.B. Highley, M. Witzberger-Krajcovic, J.C. Ayoob, E.C. Furbee, J.S. Minden, and S. Zappe., Lab on a Chip,
- **369** 2012, **12.22**, 4911-4919.
- 370 31 C.C. Mello, J.M. Kramer, D. Stinchcomb, and V. Ambros, *The EMBO journal*, 1991, **10.12**, 3959-3970.

- 371 32 T.C. Evans, WormBook, http://www.wormbook.org.
- 372 33 A.K. Corsi, B. Wightman, and M. Chalfie, *Genetics*, 2015, **200.2**, 387-407.
- 373 34 M. Rahimi, S. Salman, and C.T. Murphy. Biophysical Journal, 2022, 121.4: 515-524.
- 374 35 S. Brenner, *Genetics*, 1974, **77.1**, 71-94.
- 375 36 J.A. Lewis, and J.T. Fleming, 1995, Methods Cell Biol., 48, 3-29
- 376 377 378 379 37 S. Berger, E. Lattmann, T. Aegerter-Wilmsen, M. Hengartner, A. Hajnal, A. deMello, and X. Casadevall i Solvas. Lab on a Chip, 2018, 18, no. 9: 1359-1368.
- 38 C.L. Gilleland, A. Falls, J. Noraky, M.G. Heiman, and M.F. Yanik, Genetics, 2015, 201.1: 39-46.